Elucidating differential nano-bio interactions of multi-walled and single-walled carbon nanotubes using subcellular proteomics

Joseph D. T. Ndika[1,*], Jukka Sund[2], Harri Alenius[1,3], Anne Puustinen[4]

[1]*Department of Bacteriology and Immunology, Medicum, University of Helsinki, Helsinki, Finland*
[2]*Systems Immunotoxicology, Finnish Institute of Occupational Health, Helsinki, Finland*
[3]*Institute of Environmental Medicine, Karolinska Institutet, Stockholm, Sweden*
[4]*Department of Clinical Chemistry, Helsinki University Hospital and University of Helsinki, Helsinki, Finland.*

[*]Corresponding author: joseph.ndika@helsinki.fi

Systems Immunology Group, Medical Faculty, University of Helsinki
Haartmaninkatu 3 (P.O. Box 21) FIN-00014 University of Helsinki, Finland
tel. +358 29 4126215

Running title:

Hazard biomarker profiling of CNT variants

ABSTRACT

Understanding the relationship between adverse exposure events and specific material properties will facilitate predictive classification of carbon nanotubes (CNTs) according to their mechanisms of action, and a safe-by-design approach for the next generation of CNTs. Mass-spectrometry-based proteomics is a reliable tool to uncover the molecular dynamics of hazardous exposures, yet challenges persist with regards to its limited dynamic range when sampling whole organisms, tissues or cell lysates. Here, the simplicity of the sub-cellular proteome was harnessed to unravel distinctive adverse exposure outcomes at the molecular level, between two CNT subtypes. A549, MRC9 and human macrophage cells, were exposed for 24h to non-cytotoxic doses of single-walled or multi-walled CNTs (swCNTs or mwCNTs). Label-free proteomics on enriched cytoplasmic fractions was complemented with analyses of reactive oxygen species (ROS) production and mitochondrial integrity. The extent/number of modulated proteoforms indicated the single-walled variant was more bioactive. Greater enrichment of pathways corresponding to oxido-reductive activity was consistent with greater intracellular ROS induction and mitochondrial dysfunction capacities of swCNTs. Other compromised cellular functions, as revealed by pathway analysis were; ribosome, spliceosome and DNA repair. Highly upregulated proteins (fold change in abundance > 6) such as, APOC3, RBP4 and INS are also highlighted as potential markers of hazardous CNT exposure. We conclude that, changes in cytosolic proteome abundance resulting from nano-bio interactions, elucidate adverse response pathways and their distinctive molecular components. Our results indicate that CNT-protein interactions might have a thus far unappreciated significance for protein trafficking, and this warrants further investigation.

Keywords

Proteomics, cytoplasm, carbon nanotubes, oxido-reductive stress, ribosome, spliceosome.

INTRODUCTION

Carbon nanotubes (CNTs) are a class of engineered nanomaterials (ENMs) that have been used in the last decade to develop applications with tremendous and promising impact in industry and medicine (De Volder et al. 2013; Sharma et al. 2015). They are tubular structures consisting of one (single-walled carbon nanotubes – swCNTs) or more (multi-walled carbon nanotubes – mwCNTs) concentric graphene cylinders. The fiber-like conformation and biodurability of rod-like CNTs are stark parallels to the infamous asbestos fibers, fueling concerns that CNTs may be harmful to the human health. Several studies in rodents reveal common pathophysiological responses following CNT or asbestiform fiber exposures, which include acute-phase inflammation, granuloma formation and development of fibrosis (Muller et al. 2005; Shvedova et al. 2005; Shvedova et al. 2008; Ma-Hock et al. 2009). According to the fiber pathogenicity paradigm, (Donaldson et al. 2013) CNT toxicity is thought to be largely mediated by its morphology and biopersistence, whereas its chemical composition plays a lesser role. This differential bioactivity of chemically similar ENMs was further explained by studies showing that, once a nanomaterial is within a physiological environment, it adsorbs proteins forming a protein corona – the composition of which reflects the nature of that environment (plasma, cell cytoplasm, respiratory tract, etc.), the nanomaterial's physicochemical attributes (size, shape, surface chemistry, etc.) and the duration of exposure (Lundqvist 2013; Monopoli et al. 2012). In other words, this eventual biological identity of a nanomaterial dictates the physiological responses it elicits, including but not limited to; transport, kinetics, accumulation, signaling and ultimately, toxicity (Cedervall et al. 2007; Sund et al. 2011; Byrne et al. 2013). We previously reported differential protein binding and cellular uptake between short mwCNT and short swCNT subtypes (Sund et al. 2011). The objectives of the current study were to investigate the implications of this differential protein interaction between these two CNT subtypes at the systemic level. Because aerosolized CNT levels of up to 331 $\mu g/m^3$ and 430 $\mu g/m^3$ have been measured in industry (Siegrist et al. 2014) and in a laboratory setting (Manke et al. 2014) respectively, inhalation is a highly relevant exposure scenario. Here, we used three cell types; human monocyte-derived macrophages – to reflect the first line of defense against foreign materials and human lung fibroblast (MRC9)/lung epithelia (A549) cell lines – to mimic the exposure route (respiratory tract lining) to CNT aerosols. We hypothesized that due to the inevitable interaction of cytoplasmic proteins and CNTs once they are taken up by cells, proteomic characterization of enriched cytoplasmic fractions will provide a simple and effective way to identify material-specific health hazard biomarkers. Selected canonical pathways that were identified as differentially susceptible to these two CNT subtypes were then validated using standard assays.

MATERIALS AND METHODS

Nanomaterials

(Short) S-Purified single-walled and S-Purified multi-walled CNTs were obtained commercially (SES Research, Houston, TX, USA). Crocidolite asbestos was provided by Pneumoconiosis Research Centre (Johannesburg, South Africa) and Carbon black (Printex 90) was a gift from Evonik Industries AG (Essen, Germany). Characterization and dispersion protocols for these materials have been established in-house and previously described; mwCNT and swCNT (Sund et al. 2011; Catalán et al. 2012), asbestos crocidolite and carbon black (Palomäki et al. 2011). In the current study, size distribution and zeta potential characterization of 1 mg/ml nanomaterial suspensions in cell culture media containing 10% FBS were carried out for CNTs as described previously (Sund et al. 2011).

Cell models and growth conditions

Human lung epithelia – A549, human lung fibroblasts – MRC9 (both cell lines from ATCC, Manassas, VA, USA) and human monocyte-derived macrophages (MDM) were used for exposures. Human MDM were differentiated from peripheral blood mononuclear cells (PBMCs) obtained from healthy blood donors (The Finnish Red Cross Blood Transfusion Service, Helsinki, Finland). The differentiation was performed by isolating peripheral blood mononuclear cells from buffy coats by Ficoll-Paque Plus - gradient low-speed centrifugation as described previously (Sund et al. 2011). The macrophage medium was changed every two days. Maturated macrophages are used for exposure studies on the seventh day. Epithelial cells (A549) and lung fibroblasts (MRC9) were both cultured in DMEM containing 2 mM L-glutamine supplemented with 10 % of heat inactivated FBS and 1% PEST antibiotics. MRC9 culture medium was additionally supplemented with 1% L-Glutamine.

Cell exposure

Prior to *in vitro* exposure, a stock suspension was made in glass tubes containing 1 mg/ml nanomaterials in their respective cell culture media, supplemented with 10% FBS. The stock was sonicated for 20 minutes and diluted to final concentrations of 300, 30 and 3 µg/ml. Cell monolayers at about 70% confluence were exposed for 24h (37^{o}C, 5% CO2) with 35 µl (96 wells plate) 400 µl (12 wells plate) or 1 ml (6 wells plate) of the desired nanomaterial, corresponding to doses of 31.5, 3.15 and 0.315 µg/cm^2. This dose range was chosen such that cells retain > 70% viability after exposures. Unexposed cells in adjacent wells were taken along as controls. After exposures, cells were washed three times with warm DPBS and harvested by trypsinization (A549, MRC9) or scraping (Macrophages).

Sample preparation for LC-MS/MS

Cell cytoplasm was enriched by ProteoJET™ Cytoplasmic and Nuclear Protein Extraction Kit (Fermentas, Waltham, MA, USA). Excess nanotubes were washed off from cell monolayers 24h after exposures. Cells were harvested and pelleted with cold PBS. Cell lysis buffer supplemented with 1X protease inhibitor cocktail (Halt™ Protease and Phosphatase Inhibitor Cocktail, EDTA-free, Thermo Fisher Scientific, Waltham, MA, USA) was then added to cell pellets and cytoplasmic protein extracts were isolated as per kit instructions. Protein concentrations were measured with a BioRad DC protein assay kit. Tryptic peptides for label free proteomics were prepared according to standard procedures.

LC-MS/MS proteomic analysis, data acquisition and label free quantitation

Each peptide mixture was analyzed by automated nanoflow capillary LC–MS/MS using a nanoLC 1000 (Proxeon, Thermo Fisher Scientific) coupled to a benchtop quadrupole orbitrap mass spectrometer (QExactive^{TM}, Thermo Fisher Scientific). Proteome quantitation was performed using a bottom up data dependent acquisition approach on a QExactive platform. Column specifications, reverse phase peptide separation on 3h gradients and MS/MS data acquisition parameters have been described (Cypryk et al. 2016). In total three independent exposures of either swCNT, mwCNT or unexposed (Control) were carried out for each cell type, followed by three LC-MS/MS injections per exposure, generating a total of 81 raw files. Label free quantitation (LFQ) was performed with the MaxQuant software (Cox et al. 2014) followed by differential abundance analysis with Perseus – a computational platform that is incorporated into the MaxQuant shotgun

proteomics pipeline (Tyanova et al. 2016). Maxquant output files containing all identified and quantified protein groups for each cell type are provided as additional files 1, 2 and 3. For analysis of differential abundance between treatment groups, 1-way ANOVA or student t test, were employed when appropriate, followed by benjamini-hochberg false discovery rate adjustment of 5%.

Pathway analyses

General pathway analysis, molecular function enrichment, annotated disease functions and canonical toxicity function enrichment was carried out in IPA (Ingenuity®, Qiagen, Hilden, Germany). Biological pathway comparison analysis was carried out for all DA proteins using the *Funrich* functional enrichment analysis software tool (Pathan et al. 2015).

Western blot validation of label free proteomics

Whole cell lysates from pelleted exposed cells were obtained by urea lysis (8M urea/100mM NaCl/10mM TrisHCl, pH8.0). Samples were normalized to same total protein concentrations with urea lysis and SDS buffers after the protein concentration of each sample was determined using the Pierce^{TM} BCA protein assay kit (Thermo Fisher Scientific). 15 µg of sample per well were loaded in 12 wells pre-cast Criterion^{TM} gels. Anti RBP4 (ab133559 - abcam) and anti SCDBP (ab155394 – abcam) antibodies were used to probe gel blots at dilutions of 1:2000(v/v) in 4% milk, overnight at 4 ^{0}C, followed by 30 min wash with 1xTBS + 0.1% Tween, and 1h incubation with1:2000 diluted secondary antibodies respectively. For ECL-based detection, blots were probed for 1h at room temperature with HRP-labelled anti-rabbit and anti-goat antibodies at dilutions of 1:2000 (v/v) in 4% milk. Protein band intensities were quantified with *Imagej* (Abràmoff et al. 2004) and expressed as log2 transformed mean ±SEM.

Adverse outcome assays

Equal cell densities were seeded into parallel 96 well plates prior to nanomaterial exposures, to have a sufficient number of wells for triplicate analyses of three independent adverse exposure outcomes. Dose-dependent changes in cell viability, reactive oxygen species (ROS) production and decrease in mitochondrial membrane potential were all measured 24h post exposure using commercially available 96 well format assays. Cell viability was determined using a CellTiter-Glo Luminescent Cell Viability Assay (Promega). Mitochondrial membrane potential was measured according to procedures described in the Mito ID^{TM} membrane potential kit (Enzo Life Sciences). Cellular ROS production was determined using a fluorescence-based 2',7' –dichlorofluorescin diacetate (DCFDA) assay (abcam, Cambridge, UK). All assay procedures were carried out as described in assay protocol, and the only slight modification was the maximum excitation and emission spectra (490 nm and 535 nm respectively) used to measure fluoregenic dichlorofluorescin. For acellular ROS production, 20 µg/ml nanomaterial suspensions were prepared in PBS. 0.03 mM DCFDA was deacetylated for 30 min at room temperature by addition of 0.01M NaOH. Deacetylated DCFDA was then added to 50 µl of nanomaterials in 96 well viewplates^{TM} at a final concentration of 0.015 mM. After incubation for 3h at 37^{0}, nanomaterial-depleted supernatant was obtained by centrifugation at 4000 rpm for 10 mins. 50 µl supernatants were transferred to fresh plates containing 100 µl PBS and dichlorofluorescin formation was measured as described above.

Availability of data and materials

The MaxQuant analysis pipeline output (identified and quantified protein groups) for each cell type (.txt files), and mass spectrometry raw files are available from the corresponding author on reasonable request.

RESULTS

Physicochemical characteristics of CNTs

The two CNT subtypes evaluated in this study have been previously extensively characterized (chemical composition, size distribution and surface charge) in similar dispersion and exposure media. Herein, we re-characterized the size distribution and surface charge in cell culture media supplemented with 10% FBS. MwCNTs had a size of 432 nm and swCNTs were found to be in the size range of 259 (33.5%) to 1393 (57%) nm. The surface charge for both CNT subtypes were similar (±0.3 mV). CNT primary size, size in dispersion, chemical composition and surface charge are outlined in Supplementary Table S1.

Effect of CNTs on cell viability

A dose-dependent decrease in cell viability was measured for all 3 cell types after 24 hours of exposure to CNTs. Exposure to similar mass concentrations of asbestos crocidolite were carried out in parallel to serve as cytotoxicity control. More than 70% viability was observed for all cell types at nanomaterial concentrations of up to 31.5 $\mu g/cm^2$ (Figure S1).

Evaluation of spatial and temporal proteome modulation

Proteomic characterization of enriched cytoplasmic fractions was carried out in cells exposed to 31.5 $\mu g/cm^2$ CNT. A total of 5353 unique protein groups were identified in all 3 cell types corresponding to 4252 protein groups in the A549 cell line, 2850 in the MRC9 cell line and 3864 in monocyte-derived macrophages. Based on Ingenuity®'s knowledgebase, 57% of all identified proteins were classified to originate from the cytoplasm. Of the remaining proteins, 5% were assigned to the extracellular space, 19% to the nucleus, 12% to the plasma membrane and 7% to other cellular compartments. Multiple sample testing at a maximum FDR of 5%, reveals the abundance of 275, 561 and 552 proteins in A549, MRC9 and macrophages, respectively, were altered by exposure to both CNTs. Principal component analysis and K-means clustering grouped all biological replicates according to the different cell and exposure types (Figure 1A and 1B). Fold change in protein abundances between exposed and unexposed cells were derived using a student's t-test (S0 of 0.5 and FDR of 0.05). Significant differentially abundant proteins identified in the mwCNT/Control and swCNT/Control, had a change in abundance ranging from 1.5- to 20-fold (Table S2). A Venn diagram distribution of these differentially abundant (DA) proteins is depicted in Figure 1C. Only 2 (APOC3, PTMS) and 3 (APOC3, NME1, IGF2) proteins are DA across all cell types in the mwCNT/Control and swCNT/Control contrasts respectively (Figure 1C). Highly upregulated proteins (> 6-fold) in response to mwCNT or swCNT exposure, for each cell type, are summarized in Table 2. Taken together, the extent of fold change in protein abundance and/or the number of differentially abundant proteins was greatest in swCNT-exposed cells (Figure 2). About 67% of all DA proteins were unique to swCNT-exposed cells and 19% to mwCNT-exposed cells. Notwithstanding, although only 14% of all DA proteins were found to be common between the mwCNT and swCNT exposures, this corresponds to 43% of the DA proteins in mwCNTs exposures, and is an indication that the adverse response to these two CNT subtypes is mediated by overlapping mechanisms.

Oxido-reductive activity, structural constituent of ribosome, and RNA binding are the main molecular dysfunctions linked to bio-CNT interactions.

In the mwCNT/Control contrast, DA proteins mapped to 50 (A549), 20 (Macrophages) and 223 (MRC9) genes and in the swCNT/Control contrast to 112 (A549), 442 (Macrophages) and 196 (MRC9) genes. Bearing in mind the apparent cell-type specificity of the molecular responses to these two CNT subtypes (Figure 1C), a comparative analysis of functionally enriched pathways was carried out on merged DA proteins from all three cell types. This approach averages out those responses that are due to specialized cell type functions, leading to a more generalizable snapshot of the cellular functions that are affected by adverse of bio-CNT interactions. DA proteins from the exposure/control contrasts in all 3 cell types mapped to a total of 942 non-redundant genes, corresponding to 273 genes in mwCNT/Control and 669 genes in swCNT/Control, of which 116 genes were common between both sets (Figure 2A).

The most enriched molecular activities together with the affected pathways are summarized in Figure 3. Key molecular activities represented by DA proteins were similar for both mwCNT and swCNT exposures, and these corresponded to ribosome structural constituents, oxidoreductase activity and RNA binding (Figure 3A). These enriched molecular functions were most associated with pathways corresponding to protein synthesis and cell morphology in mwCNT exposures, with free radical scavenging and cellular assembly/organization in swCNT exposures and with cell death/survival and post-transcriptional modifications in both exposures (Figure 3B). Based on the direction of fold change in protein abundance, the top-most predicted disease endpoints were associated with increased cell proliferation and decreased DNA repair ability. Inflammation (LXR/RXR and FXR/RXR), cell proliferation and fibrosis, were most significantly enriched as top disease and toxicological functions in DA proteins from the swCNT exposures (Figure 3). Mitochondrial dysfunction was the most enriched toxicity related outcome for both of these CNTs. The p-value for enrichment of DA proteins corresponding to mitochondrial dysfunction was most significant in the swCNT exposures. To shed more light on the distinctive bioactivities between these CNT subtypes we performed a comparison analysis of the top common biological pathways represented by all DA proteins and then separately for downregulated and upregulated proteins (Figure 4). For these comparison analyses, two criteria were employed; the percentage of DA proteins from the input dataset (mwCNT/Control or swCNT/Control) that mapped to a specific pathway was used to infer the relative importance of that pathway amongst all the pathways triggered by the same input genes and the number of DA proteins was used to infer the relative potency with which a specific pathway was affected by each of the two CNT subtypes. The top shared pathways that were differentially represented by all DA proteins from the mwCNT and swCNT exposures were; diabetes pathways, translational regulation, mRNA processing pathways and respiratory electron transport. Amongst these four, the most similar pathway between the two exposures was the respiratory electron transport system of the mitochondria, which was affected by about 15% of DA proteins from both exposures. However, this corresponded to around 40 DA proteins in the mwCNT exposures and 106 DA proteins in the swCNT exposures (Figure 4A). The greatest differential representation among the top pathways was observed for ribosome-associated pathways (translation elongation, formation of free 40s subunits, etc.) and spliceosome-associated pathways (mRNA splicing, mRNA transcript formation and maturation, pre-mRNA processing). The ribosome was predominantly modulated by mwCNTs (31% mwCNT vs. 3% swCNT), and the spliceosome by swCNTs (11% swCNT vs. 3% mwCNT) – Figure 4A. Further stratification of all DA proteins into downregulated and upregulated proteins for each exposure type reveal that the bulk of proteins representing the spliceosome were downregulated following CNT exposure (Figure 4B), while the reverse held true for biological pathways relating to ribosomal function (Figure 4C). Interestingly, although the ratio of DA proteins corresponding to the respiratory electron transport system was comparable for both exposures, none of the DA proteins from this pathway were downregulated in mwCNT/Control, as opposed to the swCNT/Control exposure wherein biological pathways indicative of mitochondrial dysfunction were biased towards downregulated proteins (Figures 4B-C and Figure S2). Other notable differentially activated pathways were; downregulation of proteins involved in induction of cell death (NF-kB, FAS and Caspase signaling), upregulation of lipid metabolism and integrin cell surface interactions.

Immunoblot validation of quantitative proteomics

To highlight the reliability of label-free proteomics quantitation, two in-house antibodies against RBP4 (retinol binding protein 4) and SDCBP (syntenin-1), were used to re-assess protein abundance levels via western blot following new rounds of exposure to 3 different doses of mwCNT and swCNT. Figure 5 depicts a side-by-side view of LC-MS/MS quantitation (0 and 31.5 $\mu g/cm^2$) and western blot validation (0, 0.315, 3.15 and 31.5 $\mu g/cm^2$). For both proteins, the direction of change in abundance following CNT exposure was similar for LC-MS/MS and western blot quantitation. Representative protein blots are also shown.

***In vitro* analysis of distinctive oxidoreductive potencies**

Based on the aforementioned comparison criteria (Figure 4), we deduced that respiratory electron transport dysfunction was the most significant pathway common to adverse exposure of both CNT subtypes, with the

single-walled variant appearing to be more potent. To validate this, we investigated ROS production capacities of both materials *in vitro* and *in vivo*, as well as their abilities to decrease mitochondrial membrane potential. Intracellular reactive oxygen species (ROS) was measured 24h post exposure to mwCNT and swCNT with asbestos crocidolite exposures as positive control. ROS production was dose-dependent in all 3 cell types (Figure 6). At all tested doses (0.315, 3.15 and 31.5 µg/cm^2) CNT-induced ROS production was greater than that in cells exposed to similar mass concentrations of asbestos (Figure 6A-C). Intracellular ROS production was similar for both CNT subtypes at 0.315 µg/cm^2, but 2- to 3-fold higher in cells exposed to 3.15 and 31.5 µg/cm^2 swCNTs. At a CNT dose of 31.5µg/cm^2, induction of intracellular ROS production over 24h was decreased by treatment of A549 cells with routinely used antioxidants; N-acetylcysteine, Pyrrolidene dithiocarbamate and Diphenyleneiodonium (Figure 6D). At the concentrations tested, these antioxidants were more effective at inhibiting ROS production in the mwCNT exposures and N-acetylcysteine was the most effective antioxidant. Only N-acetylcysteine significantly inhibited ROS production in the swCNT exposure. To answer whether material chemistry or unknown contaminants could explain these differences in intracellular ROS production, cell-free ROS generation at nanomaterial concentrations of 20 µg/ml was examined for each material. Carbon black – a nano-sized particle composed entirely of carbon was included as a chemical composition analogue of CNTs. Cell-free ROS production was comparable for both mwCNTs and swCNTs and only around 1.5 times less than that produced from carbon black. Surprisingly, acellular ROS production by asbestos crocidolite was about 10 times less when compared to these CNTs (Figure 6E). 24h after exposure to each material, a decrease in mitochondrial membrane potential (↓MMP) was observed at all tested doses. ↓MMP was most prominent in Macrophages and MRC9. SwCNTs were found to be the most potent inducers of ↓MMP. A dose-dependent ↓MMP in all 3 cell types was only observed for the swCNT exposures (Figure 7).

DISCUSSION

Although i*n vitro* assays remain highly relevant as initial screens to predict ENM risk and prioritize the degree of testing for *in vivo* studies,(Godwin et al. 2015) it is not straightforward to derive organism-level health impact assessment from *in vitro* models. We exposed multiple cell types with relevance to inhaled CNTs, and, by combining their unique proteomic responses, we obtained a more generalizable view of the systemic effects of adverse CNT exposure, than if investigating only one cell type. At 1 – 5 µm in length, these nanotubes fit the current description of "short" nanotubes, defined to be less than 10 – 15 µm in length.(Bernstein 2007) In concordance with earlier studies, these short(er) CNTs are mildly cytotoxic, requiring very high concentrations to decrease cell viability by more than 50% (Palomäki et al. 2010; Catalán et al. 2012). A greater than 50% reduction in cell viability was seen only in macrophages exposed to 315 µg/cm^2 swCNTs (Figure S1). A 10-fold lower dose (31.5 µg/cm^2), at which greater than 70% viable was retained in all exposures was used to elucidate systemic differences in adverse CNT response pathways between mwCNTs and swCNTs. For consistency, the same dispersion protocols with previously published studies comparing the same materials were used (Sund et al. 2011; Catalán et al. 2012). We analyzed the cytoplasm for two main reasons; firstly, subcellular proteome characterization has the appeal of its decreased sample complexity which results in improved depth of characterization as opposed to the entire cellular proteome. Secondly, once within a cellular environment, CNTs are exposed to the cytoplasm and encompassing macromolecular complexes, wherein protein synthesis, modification and trafficking take place. Whilst global protein abundance profiles might reflect a pathophysiological state, they are incomprehensive from a mechanistic point of view as other facets of protein regulation like changes in spatial distribution are largely missed. To take advantage of this we used a gentle cytoplasmic fraction enrichment method, which leaves other cellular organelles intact.

Previous studies have reported that CNTs have an extremely high affinity for cell lysate cytoskeletal proteins (Sund et al. 2011; Cai et al. 2013). Because cytoskeletal proteins are highly relevant for intracellular and vesicular trafficking (Rogers & Gelfand 2000; McGinnis et al. 2002; Caviston & Holzbaur 2006), this supports our findings that specialized macromolecular complexes that require multiprotein assembly and targeting, like the ribosome and spliceosome, were affected by CNT exposure. Competitive binding of cytoskeletal proteins to CNTs could be one of the ways that they affect the spatial distribution and function of these multiprotein complexes. There have thus far, been no reports about CNTs inducing ribosome and spliceosome dysfunction. Nonetheless, several studies have contradicted the long-standing notion that ribosomal proteins serve 'housekeeping' functions, as they have been found to be deregulated in several cancers (Naora & Naora 1999; Kreunin et al. 2007; Khimani et al. 2005; Xue & Barna 2012; Sulima et al. 2014). Alternative mRNA splicing, mediated by a complex of highly conserved proteins, termed the spliceosome, is a recognized gene regulatory mechanism with important implications for tumor onset and progression, (van Alphen et al. 2009) as well as in controlling the magnitude and duration of innate immune responses (Carpenter et al. 2014). The spliceosome was also identified as an enriched pathway in a toxicogenomics study investigating cytotoxicity induced by DNA damage in zebrafish cell lines (Li et al. 2016). Depending on their physicochemical attributes and degree of dispersion, CNTs can penetrate cells via diffusion, endocytosis or phagocytosis (Raffa et al. 2009). Both CNT subtypes are short but differ in size, surface area, diameter/length ratios, protein binding affinities and hence most likely, cellular uptake efficiencies (Table S1). It is plausible that in addition to its higher aspect ratio, the smaller swCNT fractions (33% with a size of 259nm) could have been more efficiently taken up by cells, conferring a greater potential to cause physical injury. Preferential modulation of the ribosome and spliceosome by mwCNTs and swCNTs respectively, could represent an extension of the differential potency between these CNT subtypes, wherein, deregulated splicing occurs downstream of altered ribosomal functioning. However, a dose-response proteomic assessment will be required to confirm this.

Increased intracellular production of reactive oxygen species (ROS) that can be counteracted by pretreatment with antioxidants has established oxidative stress as a hallmark of CNT-induced toxicity (Shvedova et al. 2012). We identified oxidative stress as a central common mechanism, governing adverse exposure to

mwCNTs and swCNTs (Figure 4A). Structurally intact mitochondria have a well-known role in balancing general oxidative status via their involvement in ROS metabolism. As such a net increase in ROS triggers a cycle whereby accumulating ROS further damages mitochondria causing more free radical production, and loss of the cells antioxidant capacity (Andreyev et al. 2005). Pathway analysis highlight that the outcome of CNT-induced ROS production was tightly linked to mitochondrial dysfunction and radical production by the mitochondrial respiratory electron transport chain, involving complex I – IV in mwCNT-exposed cells and complex I – V in swCNT-exposed cells (Figure S2). The greater potency of intracellular ROS induction by swCNTs is in line with observations that antioxidant treatment was more adept at decreasing ROS production in mwCNT-exposed cells than cells exposed to swCNTs (Figure 6D), and on a systemic level, proteins representative of mitochondrial dysfunction were most enriched in swCNT-exposed cells (Figures 3 and 4). Consistently EGFR1, TNF alpha and NF-kB signaling, often associated with altered ROS homeostasis, inflammasome signaling and fibrosis, within the context of adverse CNT exposures (Vietti et al. 2016) were also enriched by DA proteins.

Particle chemical composition indicate that both CNTs primarily consist of C (> 99%). This chemical composition similarity, is mirrored by their intrinsic oxidative potential (Figure 6E), which is more comparable to cell-free ROS levels generated by carbon black (100% C content) as opposed to that produced by asbestos crocidolite [$NaFe_3^{2+}Fe_2^{3+}Si_8O_{22}(OH)_2$]. Iron ions localized to the surface of asbestos are responsible for cell-free ROS production (Liu et al. 2013) however there isn't any consensus in the scientific literature with regards to abiotic ROS production by CNTs and it remains unclear if and how nano forms of carbon generate cell-free ROS. Regardless, nanoparticles have been observed to exhibit distinctly different properties from their bulk counterparts (Oberdörster et al. 2007). In agreement with our cell-free ROS data, metal ion independent radical production has also been observed for multi-walled CNTs and carbon black (Muller et al. 2008; Nymark et al. 2014). Absence of intrinsic ROS-producing capacity by CNTs has been documented in several studies (Shvedova et al. 2012) meaning that our cell-free ROS data must be interpreted with caution.

As there is no nanomaterial "exposure disease" per se, current surveillance and epidemiological studies are in most cases not specific to individual types of ENMs. Hazard markers are thus required for assessment of adverse exposure to specific materials. Only 1 protein was affected by both CNT subtypes in all 3 cell types – APOC3 (Apolipoprotein C-III). APOC3 was consistently upregulated (5- to 15-fold) in response to both mwCNT and swCNT in all 3 cell types. APOC3 and associated lipoproteins have been identified as key components of the protein corona of silica nanoparticles (Tenzer et al. 2013; Ritz et al. 2015). In this dataset, in addition to APOC3, the apolipoproteins; APOA2, APOB, APOC2, APOD and APOH were upregulated in response to CNT exposure (Table 1 and Table S2). Elevated APOC3 is associated with hyperlipidemia and an increased risk of developing cardiovascular disease (Norata et al. 2015).Since upregulated APOC3 levels are also associated with metabolic syndrome and type 2 diabetes mellitus, it is worthy to mention that APOC3 was most abundantly upregulated (14-fold) in macrophages exposed to swCNT, and incidentally, the most upregulated protein in this study was INS – upregulated more than 20-fold in macrophages exposed to swCNT. Hypersecretion of insulin occurs in response to insulin resistance (metabolic syndrome) as well in response to ER stress (reviewed in Salvadó et al. 2016). In total, 92 and 23 proteins involved in insulin synthesis and processing were DA in the mwCNT/Control and swCNT/Control exposures respectively (Figure 4A). One of these proteins - retinol binding protein 4 (RBP4), is amongst the proteins that we have validated by western blotting in this study. NME1 and SMAP1 are the only proteins that are differentially regulated in response to swCNT in all 3 cell lines. NME1 – Nucleoside Diphosphate Kinase 1, was found to be 3- to 11-fold downregulated in response to swCNT exposure. NME1 is responsible for synthesis of nucleoside triphosphates other than ATP, and is a well-described metastasis suppressor gene (McCorkle et al. 2014). SMAP1 – stromal membrane associated protein 1, is a GTPase activating protein whose overexpression has been shown to regulate clathrin-dependent endocytosis in Hela cells (Tanabe et al. 2005). SMAP1 is about 3-fold downregulated in A549 and MRC9 cells but then 8-fold upregulated in primary macrophages. PTMS

(parathymosin) was the only protein that was upregulated (3- to 9-fold) uniquely in response to mwCNT exposure in all three cell types. In a study examining the global effects of toxic metals on gene expression, *PTMS* transcripts were found to be 2-fold upregulated (Andrew et al. 2008). Another protein worth mentioning is HIG1 hypoxia inducible domain family, member 1A (HIGD1A). HIGD1A, required for morphological and functional integrity of the mitochondria (Hayashi et al. 2012; An et al. 2013), was 4-fold downregulated in response to mwCNT exposure in A549 cells and 5-fold upregulated in response to swCNT in primary macrophages and MRC9 cells.

CONCLUSION

In the current study, evaluation of adverse exposure events at the cellular and molecular level shed more light on the health hazard of carbon nanotubes. We identified systemic similarities and differences in the pathotoxicological responses of two well-characterized CNT subtypes. In addition, some of the highly upregulated proteins could be developed into exposure-specific hazard markers. Recognized toxicants like asbestos crocidolite (Panduri et al. 2003; Huang et al. 2012; Nymark et al. 2015) and long needle-like mwCNTs (Wang et al. 2012; Nymark et al. 2015) have been shown to cause mitochondrial dysfunction by inducing a decrease in mitochondrial membrane potential (↓MMP). It is interesting to observe that these shorter CNTs that we found to be mildly cytotoxic, decreased the MMP to levels that were comparable with asbestos crocidolite. Although high aspect ratio seems to be the closest correlate to CNT-induced cytotoxicity, their biodurability demands that the hazard potential of low aspect ratio CNTs should not be ignored. Here-in we show how CNT-induced ROS production is closely associated with mitochondrial dysfunction, and the molecular components thereof. As a second highlight of this study, we propose two additional paradigms (ribosome and spliceosome functionality) through which adverse exposure to CNTs can be additionally explored. Just like the mitochondrion, the ribosome and spliceosome are central macromolecular complexes with high relevance for overall cellular homeostasis and proliferation state. Taken together, our data reveal that short rod-like CNTs still represent a health hazard, and for rod-like CNTs of similar length, the single-walled variant may represent a higher toxicity propensity, the potential of which could be manipulated by increasing the number of graphene layers. From a technical point of view, we have also shown that analysis of cytoplasmic proteome abundance provides sufficient mechanistic insight to distinguish similar CNT subtypes with the added benefit of being easier to characterize than whole cell lysates.

ACKNOWLEDGEMENTS

Funding for this work was provided by the Institute of Occupational Health, Helsinki, Finland

DECLARATION OF INTEREST STATEMENT

The authors report no conflicts of interest

REFERENCES

Abràmoff, M.D., Magalhães, P.J. & Ram, S.J., 2004. Image processing with imageJ. *Biophotonics International*, 11(7), pp.36–41.

van Alphen, R.J. et al., 2009. The spliceosome as target for anticancer treatment. *Br J Cancer*, 100(2), pp.228–232.

An, H.-J. et al., 2013. Higd-1a interacts with Opa1 and is required for the morphological and functional integrity of mitochondria. *Proceedings of the National Academy of Sciences of the United States of America*, 110(32), pp.13014–9.

Andrew, A.S. et al., 2008. Genomic and Proteomic Profiling of Responses to Toxic Metals in Human Lung Cells. *Environmental Health Perspectives*, (6), pp.825–838.

Andreyev, a Y., Kushnareva, Y.E. & Starkov, a a, 2005. Mitochondrial metabolism of reactive oxygen species. *Biochemistry. Biokhimiia*, 70(2), pp.200–214.

Bernstein, D.M., 2007. Synthetic Vitreous Fibers: A Review Toxicology, Epidemiology and Regulations. *Critical Reviews in Toxicology*, 37(10), pp.839–886.

Byrne, H.J. et al., 2013. The bio-nano-interface in predicting nanoparticle fate and behaviour in living organisms: towards grouping and categorising nanomaterials and ensuring nanosafety by design. *BioNanoMaterials*, 14(3–4), pp.195–216.

Cai, X. et al., 2013. Characterization of carbon nanotube protein corona by using quantitative proteomics. *Nanomedicine : nanotechnology, biology, and medicine*, 9(5), pp.583–593.

Carpenter, S. et al., 2014. Post-transcriptional regulation of gene expression in innate immunity. *Nature reviews. Immunology*, 14(6), pp.361–76.

Catalán, J. et al., 2012. Induction of chromosomal aberrations by carbon nanotubes and titanium dioxide nanoparticles in human lymphocytes in vitro. *Nanotoxicology*, 6(September 2011), pp.825–36.

Caviston, J.P. & Holzbaur, E.L.F., 2006. Microtubule motors at the intersection of trafficking and transport. *Trends in Cell Biology*, 16(10), pp.530–537.

Cedervall, T. et al., 2007. Understanding the nanoparticle-protein corona using methods to quantify exchange rates and affinities of proteins for nanoparticles. *Proceedings of the National Academy of Sciences of the United States of America*, 104(7), pp.2050–2055.

Cox, J. et al., 2014. MaxLFQ allows accurate proteome-wide label-free quantification by delayed normalization and maximal peptide ratio extraction.

Cypryk, W. et al., 2016. Proteomic and bioinformatic characterization of extracellular vesicles released from human macrophages upon influenza A virus infection. *Journal of Proteome Research*, p.acs.jproteome.6b00596.

Donaldson, K. et al., 2013. Pulmonary toxicity of carbon nanotubes and asbestos - similarities and differences. *Advanced drug delivery reviews*, 65(15), pp.2078–86.

Godwin, H. et al., 2015. Nanomaterial Categorization for Assessing Risk Potential To Facilitate Regulatory Decision-Making. *ACS Nano*, 9(4), pp.3409–3417.

Hayashi, H. et al., 2012. HIG1, a novel regulator of mitochondrial γ-secretase, maintains normal mitochondrial function. *The FASEB Journal* .

Huang, S.X.L. et al., 2012. Mitochondria-Derived Reactive Intermediate Species Mediate Asbestos Induced Genotoxicity and Oxidative Stress – Responsive Signaling Pathways. *Environ Health Perspect*, 120(6), pp.840–847.

Khimani, A.H. et al., 2005. Housekeeping genes in cancer: Normalization of array data. *BioTechniques*, 38(5), pp.739–745.

Kreunin, P. et al., 2007. Differential expression of ribosomal proteins in a human metastasis model identified by coupling 2-D liquid chromatography and mass spectrometry. *Cancer Genomics and Proteomics*, 4(5), pp.329–339.

Li, Z. et al., 2016. RNA sequencing provides insights into the toxicogenomic response of ZF4 cells to methyl

methanesulfonate. *Journal of Applied Toxicology*, 36(1), pp.94–104.

Liu, G., Cheresh, P. & Kamp, D.W., 2013. Molecular basis of asbestos-induced lung disease. *Annual review of pathology*, 8, pp.161–87.

Lundqvist, M., 2013. Nanoparticles: Tracking protein corona over time. *Nature Publishing Group*, 8(October), pp.1–2.

Ma-Hock, L. et al., 2009. Inhalation toxicity of multiwall carbon nanotubes in rats exposed for 3 months. *Toxicological Sciences*, 112(2), pp.468–481.

Manke, A. et al., 2014. Effect of fiber length on carbon nanotube-induced fibrogenesis. *International journal of molecular sciences*, 15(5), pp.7444–61.

McCorkle, J.R. et al., 2014. The metastasis suppressor NME1 regulates expression of genes linked to metastasis and patient outcome in melanoma and breast carcinoma. *Cancer Genomics and Proteomics*, 11(4), pp.175–194.

McGinnis, J.F. et al., 2002. Cytoskeleton participation in subcellular trafficking of signal transduction proteins in rod photoreceptor cells. *Journal of Neuroscience Research*, 67(3), pp.290–297.

Monopoli, M.P. et al., 2012. Biomolecular coronas provide the biological identity of nanosized materials. *Nature Nanotechnology*, 7(12), pp.779–786.

Muller, J. et al., 2005. Respiratory toxicity of multi-wall carbon nanotubes. *Toxicology and Applied Pharmacology*, 207(3), pp.221–231.

Muller, J. et al., 2008. Structural Defects Play a Major Role in the Acute Lung Toxicity of Multiwall Carbon Nanotubes: Toxicological Aspects. *Chemical Research in Toxicology*, 21(9), pp.1698–1705.

Naora, H. & Naora, H., 1999. Involvement of ribosomal proteins in regulating cell growth and apoptosis: Translational modulation or recruitment for extraribosomal activity? *Immunology and Cell Biology*, 77(December 1998), pp.197–205.

Norata, G.D. et al., 2015. Apolipoprotein C-III: From Pathophysiology to Pharmacology. *Trends in Pharmacological Sciences*, 36(10), pp.675–687.

Nymark, P. et al., 2015. Extensive temporal transcriptome and microRNA analyses identify molecular mechanisms underlying mitochondrial dysfunction induced by multi-walled carbon nanotubes in human lung cells. *Nanotoxicology*, 5390(September), pp.1–12.

Nymark, P. et al., 2014. Free radical scavenging and formation by multi-walled carbon nanotubes in cell free conditions and in human bronchial epithelial cells. *Particle and Fibre Toxicology*, 11(1), pp.1–18.

Oberdörster, G., Stone, V. & Donaldson, K., 2007. Toxicology of nanoparticles: A historical perspective. *Nanotoxicology*, 1(1), pp.2–25.

Palomäki, J. et al., 2010. Engineered nanomaterials cause cytotoxicity and activation on mouse antigen presenting cells. *Toxicology*, 267(1–3), pp.125–31.

Palomäki, J. et al., 2011. Long, needle-like carbon nanotubes and asbestos activate the NLRP3 inflammasome through a similar mechanism. *ACS Nano*, 5(9), pp.6861–6870.

Panduri, V. et al., 2003. The mitochondria-regulated death pathway mediates asbestos-induced alveolar epithelial cell apoptosis. *American Journal of Respiratory Cell and Molecular Biology*, 28(2), pp.241–248.

Pathan, M. et al., 2015. FunRich: An open access standalone functional enrichment and interaction network analysis tool. *Proteomics*, 15(15), pp.2597–2601.

Raffa, V. et al., 2009. Physicochemical properties affecting cellular uptake of carbon nanotubes. *Nanomedicine*, 5(1), pp.89–97.

Ritz, S. et al., 2015. The Protein Corona of Nanoparticles: Distinct Proteins Regulate the Cellular Uptake. *Biomacromolecules*, p.150320125141006.

Rogers, S.L. & Gelfand, V.I., 2000. Membrane trafficking, organelle transport, and the cytoskeleton. *Current Opinion in Cell Biology*, 12(1), pp.57–62.

Salvadó, L. et al., 2016. Targeting endoplasmic reticulum stress in insulin resistance. *Trends in Endocrinology*

& Metabolism, 26(8), pp.438–448.

Sharma, A. et al., 2015. A Review on Current Carbon Nanomaterials and Other Nanoparticles Technology and Their Applications in. , 4(12), pp.1088–1113.

Shvedova, A.A. et al., 2008. Inhalation vs. aspiration of single-walled carbon nanotubes in C57BL/6 mice: inflammation, fibrosis, oxidative stress, and mutagenesis. *American Journal of Physiology - Lung Cellular and Molecular Physiology*, 295(4), pp.L552–L565.

Shvedova, A.A. et al., 2012. Mechanisms of carbon nanotube-induced toxicity: Focus on oxidative stress. *Toxicology and Applied Pharmacology*, 261(2), pp.121–133.

Shvedova, A.A. et al., 2005. Unusual inflammatory and fibrogenic pulmonary responses to single-walled carbon nanotubes in mice. *Am J Physiol Lung Cell Mol Physiol*, 289, pp.L698-708.

Siegrist, K.J. et al., 2014. Genotoxicity of multi-walled carbon nanotubes at occupationally relevant doses. *Particle and Fibre Toxicology*, 11(1), p.6.

Sulima, S.O. et al., 2014. Bypass of the pre-60S ribosomal quality control as a pathway to oncogenesis. *Proceedings of the National Academy of Sciences of the United States of America*, 111(15), pp.5640–5.

Sund, J. et al., 2011. Proteomic characterization of engineered nanomaterial-protein interactions in relation to surface reactivity. *ACS Nano*, 5(6), pp.4300–4309.

Tanabe, K. et al., 2005. G Protein-coupled Receptor Kinase 2–mediated Phosphorylation of Ezrin Is Required for G Protein- coupled Receptor–dependent Reorganization of the Actin Cytoskeleton. *Molecular biology of the cell*, 16(8), pp.1–13.

Tenzer, S. et al., 2013. Rapid formation of plasma protein corona critically affects nanoparticle pathophysiology. *Nature nanotechnology*, 8(10), pp.772–81.

Tyanova, S. et al., 2016. The Perseus computational platform for comprehensive analysis of (prote)omics data. *Nat Meth*, 13(9):pp.731-40.

Vietti, G., Lison, D. & van den Brule, S., 2016. Mechanisms of lung fibrosis induced by carbon nanotubes: towards an Adverse Outcome Pathway (AOP). *Particle and fibre toxicology*, 13(1), p.11.

Vippola, M. et al., 2009. Preparation of nanoparticle dispersions for in-vitro toxicity testing. *Human & experimental toxicology*, 28(6–7), p.377—385.

De Volder, M. et al., 2013. Carbon nanotubes: present and future commercial applications. *Science*, 339(February), pp.535–9.

Wang, X. et al., 2012. Multi-walled carbon nanotubes induce apoptosis via mitochondrial pathway and scavenger receptor. *Toxicology in Vitro*, 26(6), pp.799–806.

Xue, S. & Barna, M., 2012. Specialized ribosomes: a new frontier in gene regulation and organismal biology. *Nature reviews. Molecular cell biology*, 13(6), pp.355–69.

FIGURES

Figure 1: Comparative profile of differentially abundant proteins across the different cell types and exposures using a cluster dendogram (A), principal component analysis (B, upper panel) and heat map (B, lower panel). In (A) *C* represents the controls or unexposed cells, while *mwCNT* and *swCNT* represent cells exposed to multi-walled and single-walled CNTs respectively. Hierarchical clustering of all differentially abundant proteins distinguishes different cell and exposure types (A). For each cell type, a principal component and heatmap analyses of the top-most differentially abundant proteins (1% FDR) reveals that in A549 and Macrophages, mwCNT-exposed cells have a greater proteome profile similarity with unexposed cells, while in MRC9 cells mwCNT exposure was more comparable with the swCNT exposure. In the heatmap mean protein abundance is represented as green (low) to red (high). Venn distribution of differentially abundant proteins (fold change ≥2) from mwCNT/Control and swCNT/Control contrasts across all 3 cell types are depicted in panel (C).

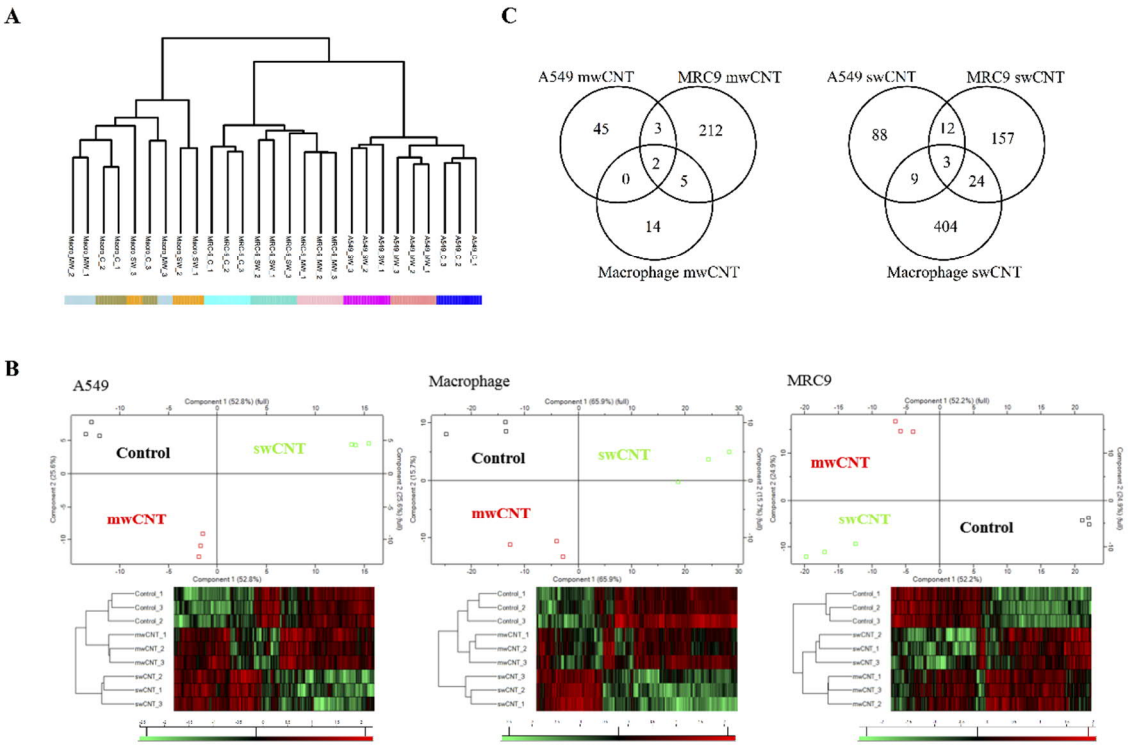

Figure 2: Number of differentially abundant proteins and degree of change in protein abundance. In total, the differentially abundant proteins from the mwCNT/Control contrast mapped to 273 genes and those in the swCNT/Control contrast to 669 genes. 116 genes were common between the two contrast sets (upper panel). In the lower panel, a plot of the number of DA proteins and the total fold change of DA proteins for each exposure type across all 3 cell types reveal a greater proteome perturbation in swCNT-exposed cells. *represents the sum of fold change in protein abundance, irrespective of direction of fold change.

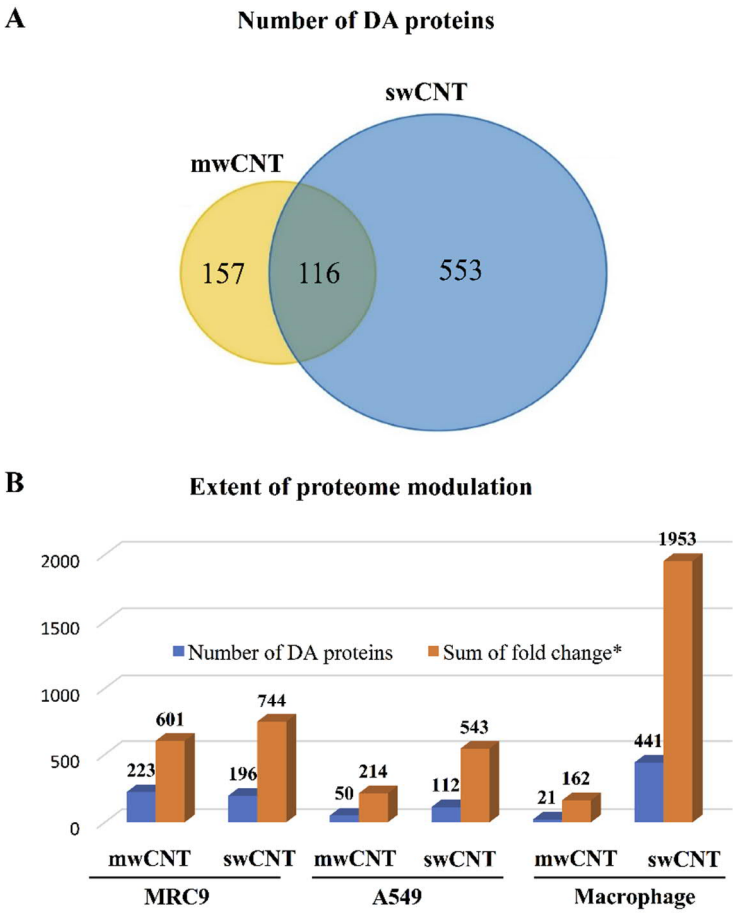

Figure 3: **Pathway analysis summary** of differentially abundant proteins from all 3 cell types.

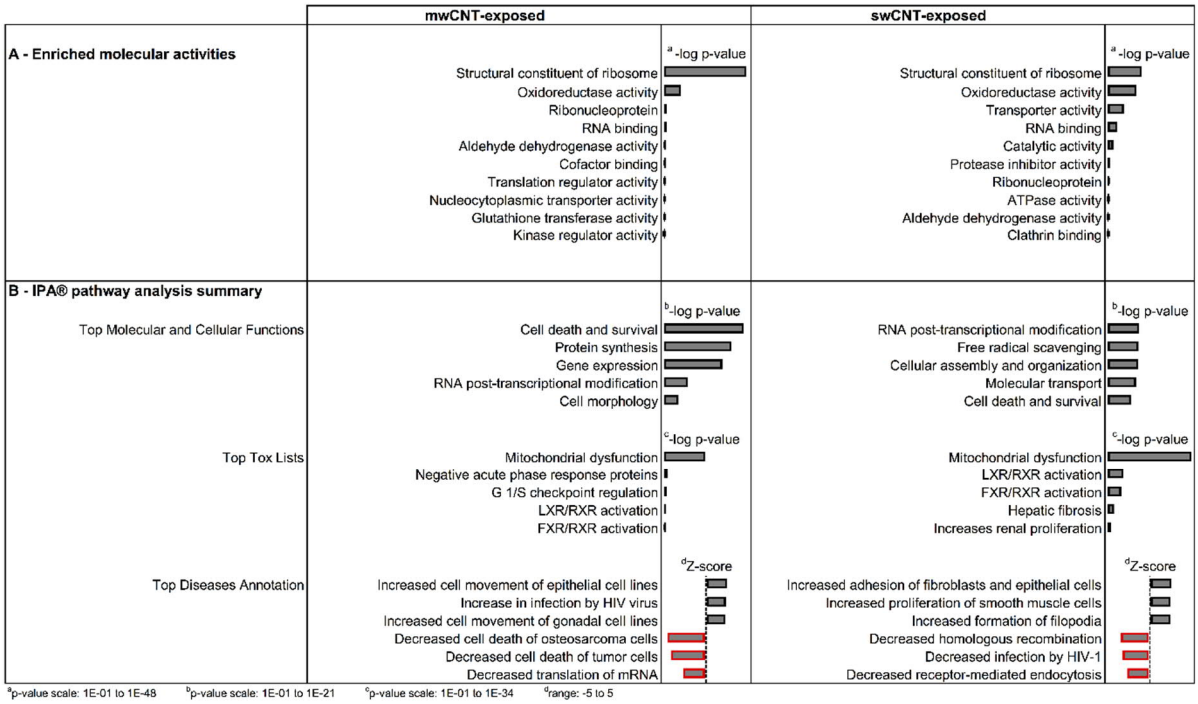

[a]p-value scale: 1E-01 to 1E-48 [b]p-value scale: 1E-01 to 1E-21 [c]p-value scale: 1E-01 to 1E-34 [d]range: -5 to 5

Figure 4: **Comparative analysis of top overlapping biological pathways.** Differential enrichment analysis of shared biological pathways between mwCNT- and -swCNT exposed cells was performed at 3 levels; using combined differentially abundant (DA) proteins from the exposure/control contrasts in all 3 cell types – i.e. 279 DA proteins in mwCNT/Control and 669 DA proteins in swCNT/Control **(A)**, using only those DA proteins that were downregulated **(B)** and upregulated **(C)** between the two contrast sets in all 3 cell types. For these analyses, the importance of a mechanism was attributed to the percentage of DA proteins from a specific pathway, within the input dataset (*heatmap on the left), while the potency of that mechanism was attributed to the total number of DA proteins representing the pathway for each contrast (**heatmap on the right). MwCNT, swCNT and C, represent mwCNT-exposed, swCNT-exposed and unexposed cells respectively. The percentage of DA proteins allocated to pathways suggestive of oxidative stress were similarly represented (about 15%) in mwCNT/C and swCNT/C, suggesting that it is an equally important mechanism of toxicity for both CNT subtypes, however, the number of DA proteins indicate that swCNTs are more potent in this regard **(A)**. In the same way, pathways suggestive of ribosomal dysfunction (translation elongation, mRNA translation, peptide chain elongation, insulin synthesis and processing) were revealed as being principal mechanisms of mwCNT-induced toxicity as opposed to mechanisms of spliceosome function (mRNA splicing, processing, maturation). The later were most activated by exposure to swCNTs **(A)**. Stratification into clusters of downregulated or upregulated DA proteins reveal that the mechanisms of toxicity triggered by mwCNT exposure are mostly mediated by upregulated proteins as opposed to swCNT-induced mechanisms of toxicity (**B** and **C**). Other common mechanisms between the two exposures were downregulation of proteins involved in caspase cascade in apoptosis (**B**), upregulation of proteins involved in lipid metabolism (**C**), both of which are more enriched in swCNT exposures.

A - Comparison of top overlapping pathways in all DA proteins

*Percentage of DA proteins (0 – 45) **Number of DA proteins (0 – 120)

Venn of all DA proteins:
160 exclusive to ***mwCNT/Control***
576 exclusive to ***swCNT/Control***
121 common in ***both sets***

	*mwCNT/C	*swCNT/C	**mwCNT/C	**swCNT/C
Diabetes pathways	36	6	100	44
Insulin Synthesis and Processing	33	3	92	23
Formation of a pool of free 40S subunits	31	3	87	18
3' -UTR-mediated translational regulation	31	3	87	18
L13a-mediated translational silencing of Ceruloplasmin expression	31	3	87	18
GTP hydrolysis and joining of the 60S ribosomal subunit	31	3	87	18
Regulation of beta-cell development	31	3	87	18
Eukaryotic Translation Initiation	31	3	87	18
Peptide chain elongation	30	2	85	16
Nonsense Mediated Decay Independent of the Exon Junction Complex	30	2	85	16
Influenza Viral RNA Transcription and Replication	30	3	85	18
The citric acid (TCA) cycle and respiratory electron transport	14	15	40	106
ATP synthesis by chemiosmotic coupling, and heat production by uncoupling proteins	14	15	40	102
Respiratory electron transport	14	13	40	92
Formation and Maturation of mRNA Transcript	3	11	9	74
Processing of Capped Intron-Containing Pre-mRNA	3	10	7	72
mRNA Splicing	3	8	7	58
Metabolism of non-coding RNA	3	4	7	25
snRNP Assembly	3	4	7	25
Transport of Mature Transcript to Cytoplasm	1	4	2	25

B - Comparison of top overlapping pathways in downregulated DA proteins

(0 – 25) (0 – 100)

Venn of downregulated DA proteins:
31 exclusive to ***mwCNT/Control***
423 exclusive to ***swCNT/Control***
40 common in ***both sets***

	mwCNT/C	swCNT/C	mwCNT/C	swCNT/C
The citric acid (TCA) cycle and respiratory electron transport	0	22	0	102
ATP synthesis by chemiosmotic coupling, and heat production by uncoupling proteins	0	22	0	100
Respiratory electron transport	0	20	0	90
mRNA Processing	6	16	4	74
Processing of Capped Intron-Containing Pre-mRNA	6	16	4	72
Formation and Maturation of mRNA Transcript	6	16	4	72
mRNA Splicing	6	13	4	58
Metabolism of non-coding RNA	9	6	7	25
snRNP Assembly	9	6	7	25
FGFR1	13	5	9	23
TNF alpha/NF-kB	13	3	9	14
snRNP Assembly	9	6	7	25
Caspase cascade in apoptosis	6	3	4	12
Loss of proteins required for interphase microtubule organizationÃ□Â from the centrosome	6	1	4	2
Transport of Mature Transcript to Cytoplasm	3	6	2	25
Cleavage of Growing Transcript in the Termination Region	3	5	2	23
flavin biosynthesis IV (mammalian)	3	1	2	2

C - Comparison of top overlapping pathways in upregulated DA proteins

(0 – 45) (0 – 100)

Venn of upregulated DA proteins:
150 exclusive to ***mwCNT/Control***
188 exclusive to ***swCNT/Control***
61 common in ***both sets***

	mwCNT/C	swCNT/C	mwCNT/C	swCNT/C
Diabetes pathways	44	12	93	30
Insulin Synthesis and Processing	41	6	86	14
Eukaryotic Translation Elongation	38	4	81	9
Formation of a pool of free 40S subunits	38	5	81	11
L13a-mediated translational silencing of Ceruloplasmin expression	38	5	81	11
3' -UTR-mediated translational regulation	38	5	81	11
GTP hydrolysis and joining of the 60S ribosomal subunit	38	5	81	11
Regulation of beta-cell development	38	5	81	11
Proteoglycan syndecan-mediated signaling events	15	33	32	82
Syndecan-2-mediated signaling events	2	7	5	18
The citric acid (TCA) cycle and respiratory electron transport	18	6	38	16
Beta3 integrin cell surface interactions	2	6	5	16
Integrin cell surface interactions	2	6	3	16
Respiratory electron transport	18	6	38	14
ATP synthesis by chemiosmotic coupling, and heat production by uncoupling proteins	18	6	38	14
Lipoprotein metabolism	2	6	5	14

DA – differentially abundant mwCNT – multi-walled carbon nanotubes swCNT – single-waled carbon nanotubes C – Control/Unexposed
* relative significance of mechanism ** potency with which mechanism is activated

Figure 5: **LC-MS/MS quantitation versus western blot analysis**. Western blot analysis was performed following triplicate 24h exposure to 0.315, 3.15 and 31.5 µg/cm^2 mwCNT and swCNT. Antibodies to RBP4 (retinol binding protein 4) and SDCBP (syntenin-1) were used to validate LC-MS/MS quantification. C denotes unexposed control cell and mwCNT/swCNT denote cells exposed to multi-walled/single-walled carbon nanotubes. 15 µg of whole cell lysate were loaded for all samples, and each sample was loaded twice, in adjacent lanes. The leftmost panel in the figure depicts log2-transformed protein abundance intensity, derived from LC-MS/MS proteomics. The rightmost panel depicts a representative blot of its expression levels as determined by western blot and the middle panel shows log2-transformed intensity-based quantitation (mean ±SEM) of western blot data. For intensity-based representation of undetected bands, an area of the blot with no detectable protein bands was selected.

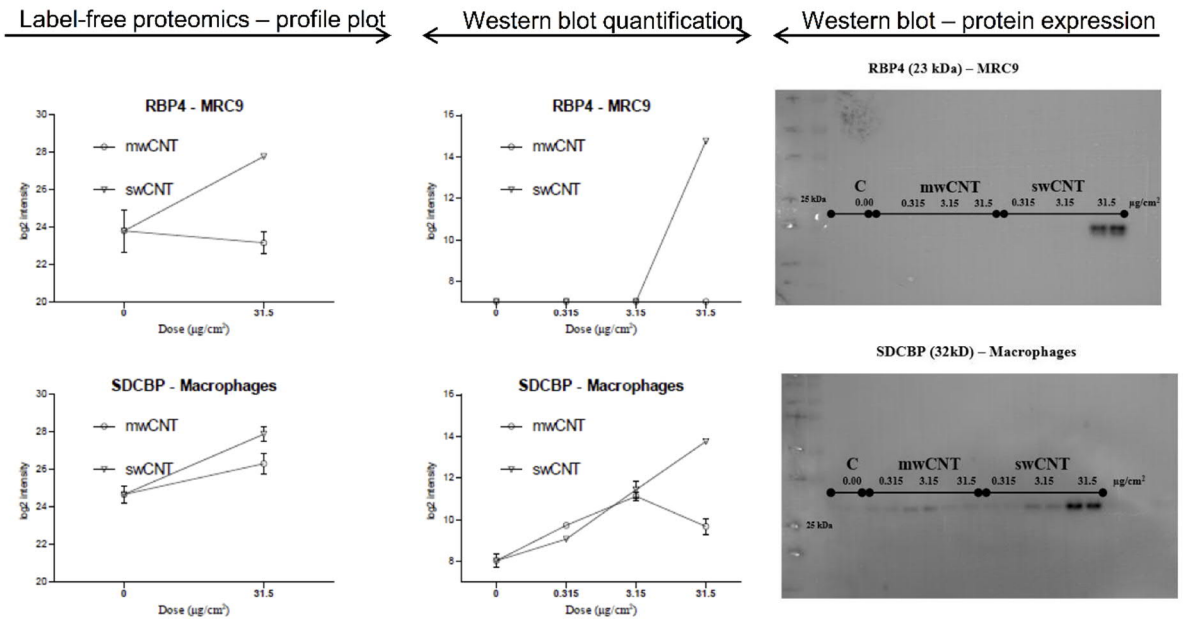

Figure 6: **Nanotube-induced ROS production**. Intracellular ROS was determined in all cell types 24 hours after exposure to mwCNT, swCNT and **A**sbestos **C**rocidolite (**A, B, C**). All 3 nanomaterials induced a dose-dependent increase in reactive oxygen species with swCNT being the most potent. Even at mass concentrations that were 10-fold higher, ROS production in cells exposed to asbestos crocidolite (315 µg/cm^2) was still significantly lower than that in cells exposed to both CNT subtypes (31.5 µg/cm^2). Cells were treated with acknowledged antioxidants – N-acetylcysteine (NAC), Pyrrolidene dithiocarbamatec (PDTC) and Diphenyleneiodonium (DPI), 1h before and during the 24h exposures (**D**). All 3 antioxidants significantly decreased ($P < 0.005$) ROS produced by exposure to mwCNT, but only NAC was able to decrease ROS induction in swCNT exposures. Acellular production of ROS was determined after 5h incubation in NaOH-deacetylated DFCH-DA, at nanomaterial concentrations of 20 µg/ml (**E**). ROS generation is quantified as the fluorescence intensity of DCF oxidized from non-fluorescent DCFH, at excitation emission/spectra of 485nm/535nm. Error bars are standard error of the mean from 4 replicates. NMs without DCFH represents the mean ROS measured from either mwCNT, swCNT or asbestos crocidolite in the absence of DCFH.

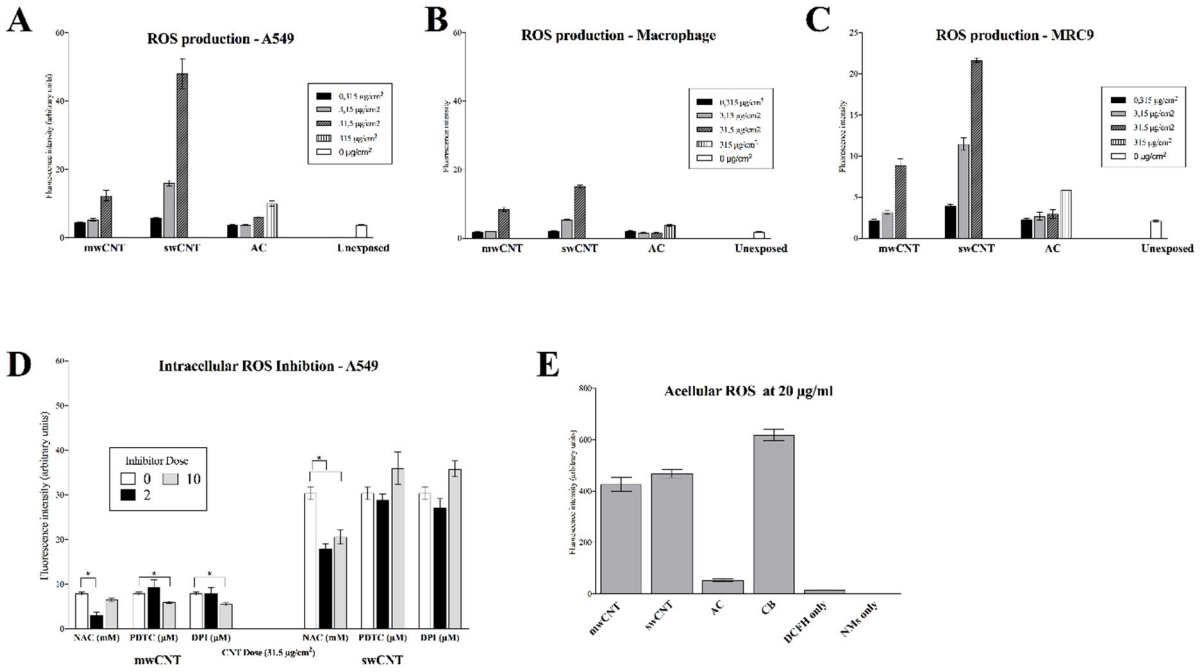

Figure 7: **Decrease in mitochondrial membrane potential (MMP)** 24h post exposure to multi-walled CNTs (mwCNT), single-walled CNTs (swCNT) and asbestos crocidolite across three cell types. Fluorescence intensities for each exposure was subtracted from that in unexposed cells. Columns represent mean and SEM of fluorescence intensity from at least 3 replicates. As positive control cells were exposed for 1h to 100µM **C**arbonyl **C**yanide 3-**C**hloro**P**henylhydrazone. Exposure to all three all materials, resulted in a significant decrease (P value < 0.05) in MMP at all the tested doses, meanwhile this decrease was dose dependent in at least 1 cell type in only swCNT and Asbestos exposed cells (P value < 0.005). In the mwCNT-exposed cells, MM depolarization observed at the lowest dose wasn't exacerbated by higher doses of mwCNTs.

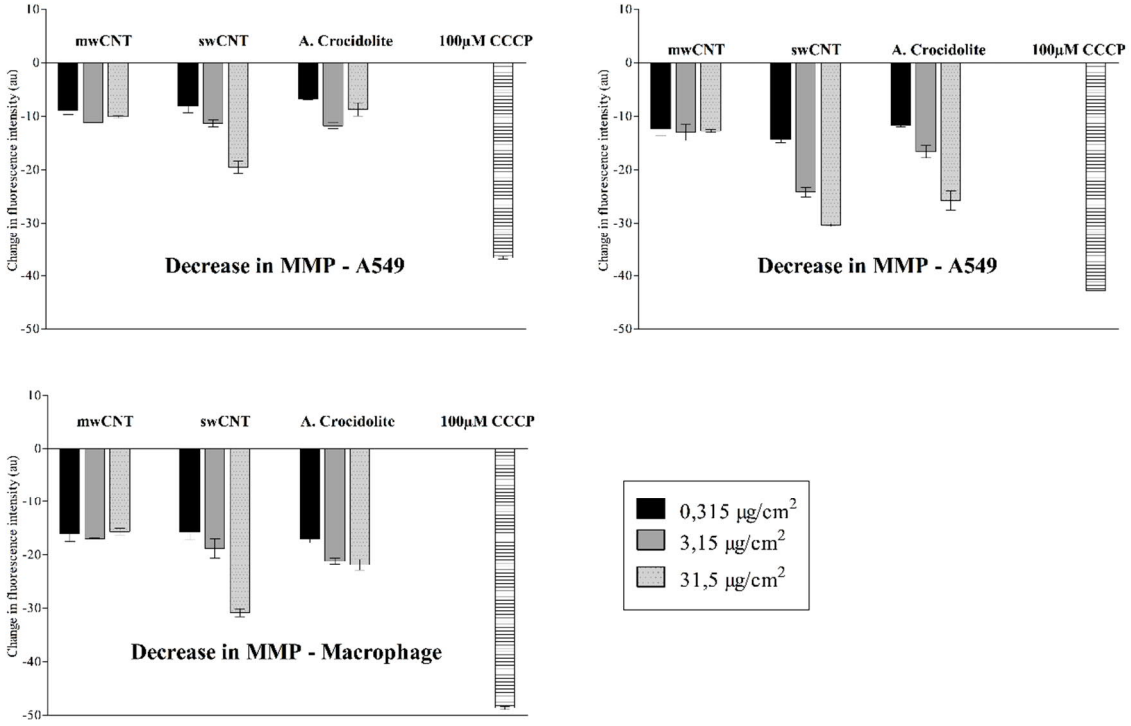

Table 1: Highly (> 6-fold) upregulated proteins

A549	**Contrast**	**Gene symbol**	**Fold change**
	mwCNT/Control	*RPL36A*	9.1
		KIAA1107	7.5
		SVIL	7.3
		NUDT4	7.3
		MRPS33	6.7
		CHMP2B	6.6
		APOC3	6.1
		KIF3C	6.1
	swCNT/Control	*FAXC*	10.3
		RBP4	7.8
		SVIL	7.7
		IGF2	7.7
		OSTC	7.3
		SMAD2	6.7
		TCEAL1	6.1
Macrophages	mwCNT/Control	*APOC3*	11.8
		PTMS	10.0
		DPM3	8.8
		APOA2	8.8
		CD99	7.6
		SMAP1	7.3
		APOD	6.5
		INS	6.1
	swCNT/Control	*INS*	20.4
		SERPINB6	15.3
		APOC3	14.1
		AHSG	13.1
		AFM	11.4
		HP;HPR	10.0
		POTEJ	9.8
		SMAP1	9.3
		PGLYRP2	9.2
		SLAMF7	9.2
		SPN	9.2
		PICALM	8.8
		APOD	8.8
		APOH	8.4
		SERPINB8	8.3
		ORM2	7.9
		A1BG	7.9
		APOA2	7.7
		ORM1	7.6
		ENTPD8	7.5
		CEP164	7.3
		HBB	7.0
		SDCBP	6.4
		NOTCH2	6.3
		SLC9A1	6.3
		CD47	6.2
		CD74	6.2
		GAL	6.2
		AMBP	6.1
		SERPINB9	6.1
MRC9	mwCNT/Control	*NPC1*	9.4
		APOC3	7.3
		TSNARE1	7.2
		HBA2	7.1
	swCNT/Control	*ITGA2*	10.2
		RBP4	8.0
		APOC3	7.5
		TSNARE1	7.1
		ITM2B	7.1
		CCDC80	6.6
		LYRM4	6.3

ADDITIONAL FILES

Figure S1: **Cell viability** (Cell Titre-Glo^{TM} luminescence assay). Cell monolayers; A549 (A), Macrophages (B) and MRC9 (C) were exposed for 24h to mwCNT, swCNT and Asbestos Crocidolite nanofibers. Percentage viability is derived from the ratio of the luminescence signal at each concentration to the average of that measured in unexposed (0 µg/cm^2) cells. Error bars are standard error of the mean from 3 technical replicates.

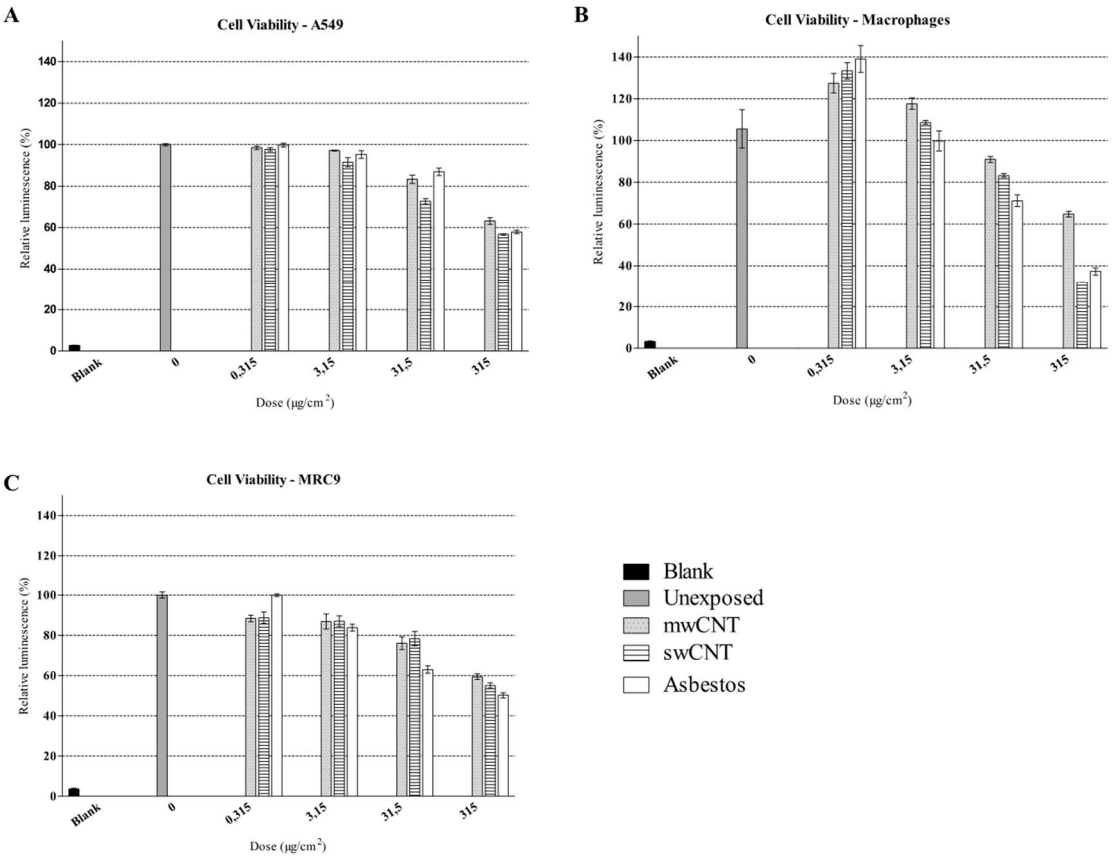

Figure S2: **Ingenuity®-derived depiction of gene mutations associated with mitochondrial dysfunction.** Downregulated proteins from our proteomics dataset are highlighted in green whilst upregulated proteins are colored red.

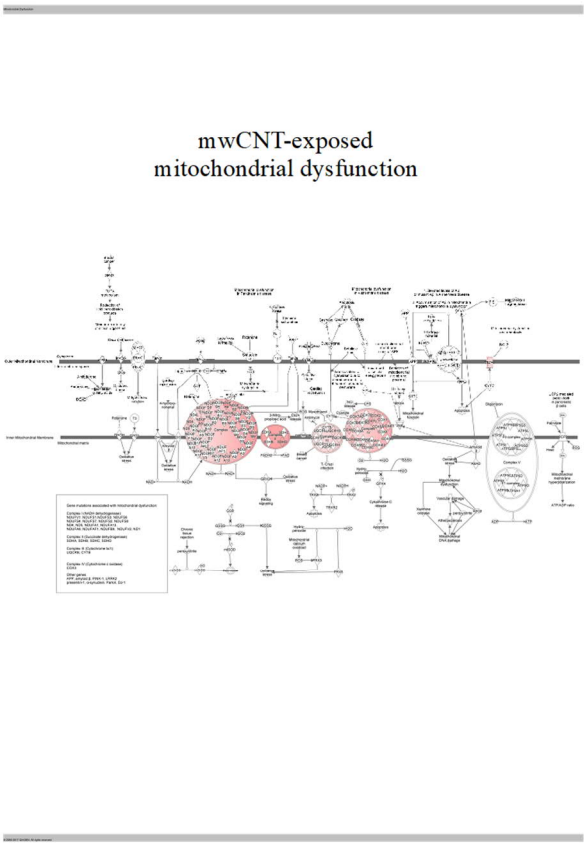

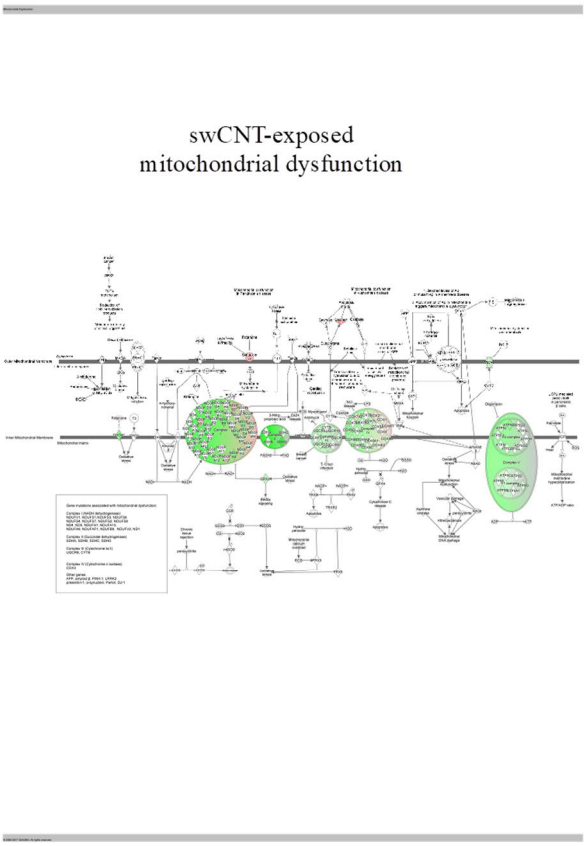

Table S1: Primary and dispersion characterized carbon nanotube physicochemical properties

Material	**Catalogue number**	**Composition(%wt.)**(1)	[a]**Primary size**	**Surface area**(2)	**Size in dispersion**	**Zeta potential in dispersion**
Short purified MWNT (**mwCNT**) SES Research	900-1260	➢ 95% nanotubes ➢ 95% MWNT ➢ < 2% amorphous C ➢ < 0.2% ash content	➢ Length: 1 – 2 µm ➢ Outer diameter: 10 – 30 nm ➢ [b]Minimum length-to-diameter ratio: 33/1	436 m^2/g	96.3%: 432 nm 3.7%: 4.4 µm	-13.35 mV
Short purified SWNT (**swCNT**) SES Research	900-1351	➢ 90% nanotubes ➢ 50% SWNT ➢ < 5% amorphous C ➢ < 2% ash content	➢ Length: 1 – 5 µm ➢ Outer diameter: < 2 nm ➢ [b]Minimum length-to-diameter ratio: 500/1	60 m^2/g	56.9%: 1.4 µm 33.5%: 259 nm 9.6%: 4.6 µm	-13.02 mV

[a]Provided by vendor (SES Research)

[b]Calculated as minimum length divided by maximum diameter

1. Sund J, Alenius H, Vippola M, Savolainen K, Puustinen A. Proteomic characterization of engineered nanomaterial-protein interactions in relation to surface reactivity. ACS Nano. 2011;5(6):4300–9.

2. Vippola M, Falck GCM, Lindberg HK, Suhonen S, Vanhala E, Norppa H, et al. Preparation of nanoparticle dispersions for in-vitro toxicity testing. Hum Exp Toxicol. 2009 Jun;28(6–7):377—385.

Table S2: List of all significant differentially abundant proteins (Upregulated and Downregulated) for each cell type

A549_mwCNT	A549_swCNT	MRC9_mwCNT	MRC9_swCNT	Macrophages_mwCNT	Macrophages_swCNT
Gene names	**Gene names**	**Gene names**	**Gene names**	**Gene names**	**Gene names**
KIAA1107	FAXC	KRTDAP	ITGA2	APOC3	INS
RPL36A	RBP4	NPC1	TSNARE1	DPM3	APOC3
SVIL	OSTC	TSNARE1	RBP4	APOA2	SERPINB6
THAP5	IGF2	APOC3	KRTDAP	CD99	AHSG
APOC3	SVIL	HBA2	APOC3	INS	PGLYRP2
KIF3C	PICALM	ASPM	ITM2B	APOD	SLAMF7
CHMP2B	DHRS11	PDE4DIP	LYRM4	SMAP1	AFM
RPS29	CAST	RPS29		PGLYRP2	ORM2
PTMS	CLDN2		ASPM	AHSG	HP
RAB3B	APOC3	CD99	BMP1	PPFIBP1	SPN
TCEAL1	DDX19B	NDUFC2	IGFBP2	CMC2	POTEJ
RPL29	TSPO	RPL34	LOX	PRDX4	APOD
GABRA5	SMAD2	NDUFA6	DARS2	H2AFV	SERPINB8
AGRN	RAB3B	CLDN11	ELP2	CPSF2	CEP164
SKA1	MTM1	MRPS7	PSIP1	COL6A5	APOH
NRG1	TCEAL1	GK	RNF213	RAB11A	SMAP1
SLC52A2	STAMBPL1	DNAJC1	HBA2	HIST1H2BL	AMBP
ABI2	DDX17	SDHD	ARAP1	H3F3A	A1BG
TCIRG1	DHX37	SRC	CCDC80	FLAD1	APOA2
COA3	MRPS33	PTMS	NDUFS2	HIST1H3A	TPM3
SPATS2	SKA1	PSIP1	GTF2A1		DPY19L1
UNC5CL	PMM1	BMP1	IGF2		HBB
BOP1	SCRN3	FXR1	SRC		PICALM
ZDHHC5	CXorf38	ERLIN1	TGFBI		CHMP5
CYSTM1	STAB1	MCU	IGFBP4		LRRFIP1
CAMK1D	H1FX	COX6B1	MRPS21		CASP3
TNFRSF10B	PTPLB	TMEM179B	WDR82		ORM1
TGFBI	SRGAP1	COX7C	NPC1		NOTCH2
EPS15	OSBPL2	MTX2	IGFBP5		SDCBP
WDR48	RBM26	RBM34	FNDC3B		ENTPD8
MSH3	UNK	PRKRA	NDUFA9		SLC9A1
SGK223	UNC5CL	TBL2	MRPS27		CD74
RPL35A	HP1BP3	STAU1	TBC1D2		IL8
UBE4A	PEG10	SZRD1	CTGF		SERPINB9
UNC119	ADD3	FAM115C	STAB1		TK2
GEMIN2	CRELD1	MRPS21	DCN		SERPING1
SMARCC1	SCD	SERINC1	VNN1		CD47
CCDC151	COMMD6	COX6C	ATP6AP2		PRDX4
	SLC25A4	NDUFB9	NDUFA13		TTR
PM20D2	EPS15	CASP7	TNC		HPX
PPP1R8	TGFBI	NDUFA9	CHID1		SERPINB1
ISCA1	GNAI1	RRBP1	TBL2		APOC2
HIGD1A	MAPK1IP1L	PRDX4	ERLIN1		CCL3

CD320	CYP24A1	NDUFS2	PPAP2B		ITM2B
LEPREL1	CLNS1A	GTF2A1	APOB		SPP1
CRADD	RFK	CLTB	RABEP2		KCMF1
FUBP1	H3F3A	MRPL37	SRP9		GAL
GEMIN6	NRP2	RECK	RPS27L		SNCA
BCL2L1	44089	FNDC3B	MT-CO2		HBA1
AKAP9	C5orf22	TBC1D2	COX7A2		BSG
	CCDC50	MT-CO2	FAM98A		C11orf58
	LRRC8C	TOMM22	DDX17		FAM175B
	PAQR5	PPAP2B	ATAD3A		TRAPPC8
	GPX1	CKAP4	ENDOD1		C16orf54
	NUDT2	PRRC2C	SLC1A4		HN1L
	TRIM4	MT-ND4	CST3		SELPLG
	DHODH	ERLIN2	FN1		WBSCR16
	TSEN54	IGF2BP3	MYADM		TYROBP
	MDP1	TFPI2	CKAP4		ASNS
	NIPA1	MRPL28	ABCD3		SERINC1
	LYRM7	RPL21	COL5A1		RCSD1
	GLRX2	RPS27L	RPS14		TFCP2
	NBN	BROMI	RPS21		P4HA2
	ALG11	TNC	RRBP1		C5AR1
	USP3	IMMT	VDAC3		GSTM3
	NME1	CHCHD3	COL1A2		C20orf27
	NUBPL	PLAUR	RPS20		TMCC3
	GOLM1	LBR	LMNA		NDFIP1
	CD320	NDUFV1	IGF2BP1		TNFAIP8
	TRAFD1	TRAM1	MTHFD1L		ETNK1
	GNB1L	RPS21	PTTG1IP		MTMR14
	SMAP1	GNB2L1	HDLBP		SQSTM1
	FKBP14	COX7A2	RPL23A		ARL2
	CHMP7	CHID1	NDUFS5		PSMB7
	FDX1	SSR4	COX4I1		SARNP
	ZFAND1	COX4I1	GNB2L1		TSC22D4
	SPTAN1	KRTCAP2	EIF3F		ZMIZ2
	CTU2	GREM1	IMMT		CENPF
	METTL3	RPL30	NT5E		HEATR5B
	CRK	RPL13A	HADH		ISCU
	MAPRE3	IKBIP	IPO4		ARL6IP5
	UBE2L6	ATAD3A	RETSAT		ARFGAP2
	SLC41A3	PTPN9	SNAPIN		PLAUR
	DHRS3	TECR	YWHAG		LPL
	XYLB	NDUFA13	SMAD3		ASMTL
	CNIH	RPS20	BDH2		EBF2
	POLRMT	YBX1	SH3BP4		BTRC
	GCC1	ATP6AP2	LMF2		GET4
	PNMA3	EIF3J	C16orf62		RANBP3
	SCAMP4	COL4A2	UQCRQ		PFKM
	MDH1	FAU	KIAA1199		HMGA1
	GABARAP	SSR1	PDCL3		NCS1
	STARD9	RPL19	APOL2		MRI1
	CCDC151	MT-ND5	RRM2B		ARFIP2

	ARFIP2	RPL11	RHOB		TRAPPC2P1
	HIGD2A	RPL14	NCDN		GPC4
		NDUFS3	ACOX1		IL1RN
	ARF3	RPL23A	DNPH1		SLC38A2
	LSM7	DAD1	HGF		ALDOC
	CHMP1B	RPS14	RAB3GAP1		BABAM1
	TPM2	TMEM147	TK1		PPFIBP1
	TUBAL3	ANXA6	GLIPR1		
	RPL29	ABCD3	DTYMK		MARCKS
	AKR1C3	FAM98A	SLC4A7		TMEM106B
	MYCBP	RECQL	SNF8		CDV3
	SLTM	IGF2BP1	DNAJC9		NAF1
	RPL28	IKBIP	COG3		IFIT5
	PFDN1	PIGT	SMIM11		DHRS4
	PCNP	RPL3	SORD		PSIP1
	DUS3L	RPS11	PTPN12		HMGCS1
	RPL34	IGF2BP2	GET4		CTSK
	ARL15	VDAC3	SDSL		MAP1LC3B
		RPL37A	TMED3		TNKS1BP1
		HDLBP	EHBP1L1		EPB41L1
		RPLP2	ELAC2		HLA-DRB1
		UQCR10	LPAR1		FRMD8
		TGFBI	ACOT13		SDCBP
		PTDSS1	RPA2		SLAIN2
		RPS8	NOL3		MAP4
		NCL	NAA25		WASF2
		RPL32	LMNB2		NRBP1
		MTHFD1L	DPP9		CAST
		RPL12	TIMM9		PLEK2
		RPL22	KIF13B		CHMP4B
		SND1	FAM162A		C9orf142
		RPL18	MCCC2		TPD52L2
		RPL28	COL4A3BP		FBXO7
		RPL4	PCBP2		CD276
		TMEM258	TAOK3		MCTS1
		RPL6	MMS19		PXN
		SEC62	RANBP2		ARF5
		RPL31	WDR26		PLEKHO2
		COX5A	DAP		CST3
		NDUFS1	CCS		PPAP2B
		EBF2	ATP6V1C1		HOOK3
		SGCD	HMBS		TWSG1
		NDUFS8	PTPRK		PFDN5
		TMED4	SERPINB7		PLA2G7
		RPL13	CBR3		EFHD2
		HSD17B11	VPS4A		CTSD
		RPL5	SMAP1		RTN1
		RPL15	RNF114		CTSH
		RPL18A	FADD		NECAP2
		RPL24	ARF3		PTPMT1
		SAMM50	COMMD9		SLC35F6

		RPS9	AKR1B10		NPL
		EIF3L	IAH1		MT-CO2
		MGST1	UBE2Q1		NDUFA5
		RPS18	ALDH1A1		SQRDL
		RPLP0	HDHD1		CYB5R1
		LRRC59	CSK		COX7A2
		RPL17	SCN5A		ALDH18A1
		KDELR3	MOV10		SLC25A13
		FUS	LPCAT1		GLG1
		NDUFA8	NCAPD2		SLC25A3
		RPS3	TUBAL3		COG7
		PLAT	ARMC9		NDUFB4
		RPL7	FUNDC2		NDUFS2
		RPL23	COL6A5		DIRC2
		YBX3	PSMG3		SLC11A2
		MYADM	AGPAT1		ST3GAL6
		GEMIN5	TBCE		SNRPB2
		RPS6	SPG20		ABCD3
		VDAC2	COASY		NNT
		RPS3A	IPO11		VDAC3
		RPL27A	RPE		NDUFS8
		EEF1G	RPL36AL		LRP1
		UFL1	PPP6R3		UQCRC1
		RPS4X	CLNS1A		ZFPL1
		RPS24	NAV1		SLC25A24
		MGST3	BPHL		PHB
		EDF1	AKR1C2		PTCD3
		UQCRC2	ATP5EP2		NDUFS1
		RPS13	HIGD1A		NDUFA4
		RPSA	ATP5G1		SLC25A11
		TRIP13	ASAP1		SFXN3
		MMS19	PRPSAP2		SLC25A20
		IPO4	HSP90AB1		NDUFA10
		SH3BP4	HAT1		RPS15
		OSTF1	PIP4K2B		SLC25A1
		CCS			COX6B1
		UBE2V2	KCMF1		MRPL12
		CLNS1A	KRT18		TMED2
		ENY2	PLAT		UQCRC2
		HSPBP1	MAP2K1		KHDRBS1
		F3	IGBP1		SLC9A6
		ATRIP	CAP1		ATP5B
		IAH1	ASCC2		SCO1
		ATP6V1F	FAM114A2		DHCR24
		TXNDC9	PTMS		VDAC1
		SLC4A7	SLC39A7		NDUFB10
		PTPN12	RPL29		MRC1
		SNF8	SPCS1		TIMM17A
		SMAP1	S100A6		PET112
		TUBB4A	NME1		MRPS34
		INPPL1	AKR1C3		ILF3

		IGBP1 AKR1B10 ASAP1 CROT RHOB WDR26 PCBP2 HADH TUBAL3 TBRG4 KRT18 PDCL3 ARF3 COL6A5 MXRA7 GLRX5 PIP4K2B RAB11A PRNP ALDH1A1 PLP2 AKR1C3 AKR1C2 CDC34 HSP90AB1 ASCC2			SLC25A6 MRPL19 PRNP AGK PUF60 NDUFA9 MTCH2 SDHC DOLK UQCR10 SMDT1 COX5B IMMT RHOT1 SAMM50 NDUFA13 CTNNBL1 CTSS COX7C LACTB MP68 UQCR11 MT-ND2 IKBKAP SDHB PCBD2 ATP5J SNRPD2 ATP5O GRSF1 TFB2M TOMM22 MRPL50 GOLGA2 ILF2 MICU1 SRSF11 HIST1H2AC DDX5 SMIM11 ADD1 GALNT2 NDUFS5 NDUFA3 PQLC1 TBRG4 MRPS18B MRPS9 MRPS16 APOO PRPF19

UQCRB
RMDN3
GIMAP1
SF3A1
CRELD1
MRPL3
PXMP4
NUCKS1
TIMMDC1
MRPS35
SLC48A1
NDUFA12
HNRPLL
NDUFB1
MRPS7
ROMO1
RDH14
TMEM199
SNRPD3
MRPL40
SLC35B1
MRPS25
NDUFA8
AMFR
HIGD2A
KDM1A
hCG_2044799
NUP214
MDH1
BCKDK
EMC8
CLCC1
TMEM126A
SRSF5
MRPL38
SF3B2
TMEM50A
MRPL46
APLP2
TLR8
NDUFV2
NDUFB8
SF3B14
ATAD1
RANBP6
STX16
SLC43A2
ATP6V0C
PET100
HNRNPA3
HSF5

					TCERG1
					MAN2B2
					AP1B1
					CEPT1
					C10orf11
					MRPL23
					GALC
					MRPL1
					SCAMP1
					SELT
					MRPL17
					TOR1AIP1
					MBP
					MFN2
					CHCHD3
					MRPL37
					ARMC10
					SF3B1
					SMU1
					MTA2
					PGAM5
					MRPL4
					SNX29
					SF3B3
					NONO
					WDR5
					VSIG4
					SRSF9
					TRIM38
					RAD50
					CLPTM1L
					LMNB2
					SUN2
					SNRPA
					NPEPL1
					DMXL1
					SLC25A35
					NDUFB11
					SLC25A19
					SNRNP70
					MRPS28
					SRSF7
					MT-ND3
					CHD4
					COX6C
					MRC2
					GLYR1
					NUP153 variant protein
					NR3C2
					GALNT7
					SRSF1

SLC26A11
TIMM23B
CPSF2
MRPL53
SLC25A12
COL6A5
MRPS26
ERH
RAE1
MRE11A
SFPQ
CHERP
SNRPD1
RPA2
AGO1
AOAH
ICMT
NFAM1
MRPL30
MTFP1
PARP10
YIPF3
MRPL32
RBMX
COA3
SNRPF
TMED4
NDUFS4
DDX21
ABHD16A
SNRPE
DHX9
MFF
HIGD1A
RMDN2
TM6SF1
CTCF
C10orf54
HNRNPC
DNMT1
FBL
DHODH
H2AFV
NDUFB6
NDUFS7
C9orf89
HIST2H3PS2
RAB11A
VMP1
HNRPDL
NDUFA2

					HIST1H2AJ GABARAP HIST1H2BL MCEMP1 SRRM2 GLIPR1 SYNE1 HIST1H4A NME1 SF3A3 LMNB1 NUP155 SLC39A7 SEPN1 HSP90AA4P DNAJC11 CPSF7 ATP5EP2 SNX14 SFRS3 MRPL47 CAMP GNPTAB HIST3H2BB DNAJA3 MATR3 NDUFB5 TOMM5 RALY NUMA1 ADAR S100A6 SPOCD1 H2AFY SDHD H3F3A HIST2H3A PDSS2 HIST1H3A